BJRS
BRAZILIAN JOURNAL OF RADIATION SCIENCES

doi.org/10.15392/2319-0612.2025.2637
2024, 12(4A) | 01-19 | e2637
Submitted: 2024-08-26
Accepted: 2024-11-19

A 3D Printing Based Anthropomorphic Eye Phantom Development

A. Fidelis[1]; D. Pereira[2]; L. da Rosa[1] and S. C. Cardoso[3]*

[1] Programa de Pós-Graduação em Radioproteção e Dosimetria (IRD/CNEN), Rio de Janeiro, Brasil.
[2] Oncologia D'or São Cristóvão - Rede D'or São Luiz, Rio de Janeiro, Brasil.
[3] Instituto de Física, Universidade Federal do Rio de Janeiro (UFRJ), Rio de Janeiro, Brasil.

*Correspondence: simone@if.ufrj.br

Abstract: This study aimed to construct a tissue-equivalent anthropomorphic phantom using 3D printing to enable dosimetry with radiochromic films of the optical apparatus in external beam radiotherapy. Slices were developed based on and intended to be used in conjunction with the reference phantom ATOM. 3D printing with polylactic acid (PLA) was utilized to represent soft tissues, while a mixture of gypsum, salt, and water was used as a skull bone simulator. The validation of the phantom was conducted through Hounsfield Units (HU) assessments to verify the homogeneity and compatibility with the ATOM phantom. Homogeneity was confirmed with a variation of 28.1% in the PLA component and 6.6% in the gypsum mixture. The results also demonstrated compatibility with the materials of the ATOM phantom. The phantom was successfully constructed and validated, making it suitable for testing as a dosimetric system for evaluating doses in the ocular region during radiotherapeutic procedures.

Keywords: Anthropomorphic phantom, Dosimetry, eye, 3D printing, Radiotherapy.

BJRS
BRAZILIAN JOURNAL OF RADIATION SCIENCES

doi.org/10.15392/2319-0612.2025.2637
2024, 12(4A) | 01-19 | e2637
Submitted: 2024-08-26
Accepted: 2024-11-19

Desenvolvimento De Um Simulador Antropomórfico De Olho Por Impressão 3D

Resumo: O objetivo deste trabalho foi a construção de um simulador antropomórfico tecido-equivalente por impressão 3D para permitir dosimetria com filmes radiocrômicos do aparelho óptico em radioterapia com feixes externos. Foram desenvolvidas fatias baseadas no simulador de referência ATOM® e que devem ser com ele utilizadas. A impressão 3D em ácido polilático (PLA) foi utilizada para representação dos tecidos moles, enquanto uma mistura de gesso, sal e água foi usada para os tecidos ósseos do crânio. A validação do simulador foi realizada por avaliações de unidades de Hounsfield (HU) para verificação de homogeneidade e compatibilidade com o simulador ATOM. A homogeneidade foi atestada ao apresentar 28.1% de variação na peça em PLA e 6.6% na mistura de gesso. Os resultados também demonstraram compatibilidade com os materiais do simulador ATOM®. O simulador foi devidamente construído e validado, podendo ser testados como sistemas dosimétricos para a avaliação das doses na região ocular nos procedimentos radioterapêuticos.

Palavras-chave: Simulador antropomórfico; Dosimetria; Olho; Impressão 3D; Radioterapia.

SBPR

1. INTRODUCTION

Ocular cancers can affect any structure of the eye in individuals of all ages. For cases recorded in individuals under 15 years of age, retinoblastoma was the most common (86%). In contrast, for those over 15 years old, melanoma was the most recurrent tumor (29%), being the most common primary ocular tumor in adults [1,2]. In adult melanoma cases, the uvea (a structure composed of the iris, ciliary body, and choroid) is the most frequently affected (83%), with the highest incidence occurring in the choroid [2]. Additionally, other types of neoplasms have a high probability of metastasizing to ocular structures, such as breast, lung, and gastrointestinal carcinomas [3,4]. Regarding incidence in Brazil, 2166 cases of uveal melanoma were recorded between 2000 and 2016, reinforcing its position as the most common primary tumor in the ocular region, accounting for 5.4% of all melanomas [5].

Estimates of 5-year mortality rates due to uveal melanoma range from 16% for small tumors to 53% for large tumors [2]. A study conducted in Brazil observed a decline in mortality rates in children due to ocular tumors between 1980 and 2002 (from 0.17/100,000 to 0.07/100,000). According to the authors, this finding can be attributed to advancements in retinoblastoma treatments [6].

As treatment methods, radiotherapy and enucleation are the most commonly used [2]. Treatments involving the application of ionizing radiation include two modalities: brachytherapy, which utilizes I-125, Ru-106, and Sr-90 plaques surgically positioned near the lesion [7,8], and external beam radiotherapy (EBRT), which uses proton beams or radiosurgery with photons produced in clinical linear accelerators [9,10]. EBRT must be carefully planned to ensure the irradiation of the entire tumor while protecting the surrounding healthy and sensitive tissues [11-14]. Thus, dosimetric studies in these types of treatments aim to ensure their quality and prevent radiation-induced complications [15-17].

The use of tissue-equivalent anthropomorphic phantoms for dosimetric evaluations is one of the major sources of research in Medical Physics. Their purpose is to mimic human biological tissues in order to study absorbed dose distributions without the need to insert dosimeters into the patient or perform *in vivo* dosimetry. For their application, the phantom must closely resemble the organ being simulated, both anatomically and in terms of radiation interaction with matter. Ideally, phantoms should exhibit the same density, electron density, and heterogeneity distribution as human organs [18-22].

The use of certain materials as tissue-equivalents requires validation according to the parameters defined by the International Commission on Radiation Units & Measurements (ICRU) Report 44 [23]. The report recommends evaluating the chemical composition, bulk and electronic densities, mass attenuation coefficient, mass stopping power, dose distributions, and Hounsfield Units (HU) of the proposed materials.

In this context, the use of 3D printing for the fabrication of phantoms for dosimetric applications is becoming increasingly common. Its application is expanding due to the versatility and freedom in modeling components, the extensive variety of materials available for printing, and the lower cost compared to commercial phantoms. Recent studies focus on the characterization and validation of 3D prints for dosimetry in radiotherapy quality control, where authors demonstrate over 95% agreement between measured and calculated data [24,25].

For radiotherapy applications, Pereira et al. (2021) validated polylactic acid (PLA), a polymer widely used in 3D printing, as a material for simulating soft tissues [26]. Subsequently, Pereira et al. (2022) developed a 3D-printed anthropomorphic eye phantom for dosimetry in EBRT using thermoluminescent dosimeters (TLDs). The authors investigated and validated a mixture of calcium sulfate with sodium chloride to simulate skull bone tissues. Combined with the 3D printing of soft tissues, it was possible to construct the complete phantom, intended to replace slices 3 and 4 of the commercial phantom ATOM. Dosimetry in the planning target volume (PTV) corresponding to

choroidal melanoma and in adjacent organs at risk (OAR) was performed with the placement of microcube TLDs [27].

The objective of this work is to model, construct, and validate slices of an anthropomorphic ocular phantom using 3D printing for dosimetry in EBRT with radiochromic films. The construction followed protocols validated in previous studies [26,27], along with the implementation of innovative dose assessment plans using the films. Validation was conducted by comparing the HU of the constructed pieces with those of the reference. The phantom aims to enable experimental evaluation of continuous dose distributions in the PTV and OARs associated with ocular radiotherapy, such as the lens and optic nerve.

2. MATERIALS AND METHODS

In the developed phantom, 3D printing with PLA simulates soft tissues, while a mixture of calcium sulfate, water, and sodium chloride simulates cranial bone tissues. The construction of the pieces is divided into four steps: 1) Acquisition and segmentation of DICOM (Digital Imaging and Communications in Medicine) files from the ATOM phantom; 2) 3D modeling of the piece; 3) 3D printing; 4) Fabrication and filling of the printed pieces with the bone-simulating mixture. Following fabrication, computed tomography (CT) of the piece was performed to analyze the homogeneity of the print and mixture and the compatibility of the HU with reference data.

2.1 STAGES OF PHANTOM CONSTRUCTION

2.1.1 DICOM Files for 3D Printing

The phantom developed in this work was based on the CT scan of the commercial anthropomorphic ATOM phantom, female adult model. It is divided into horizontal slices with a standardized thickness of 2.5 cm to allow for the placement of dosimeters in cavities

along its structure (Fig. 1). Only the head portion was used (Fig. 1A) for acquiring the DICOM file from the tomographic image (Fig. 1C).

Figure 1 : Images of the ATOM Anthropomorphic Phantom. (A) Head ; (B) Phantom slice ; (C) Image obtained from the computed tomography of the ATOM phantom.

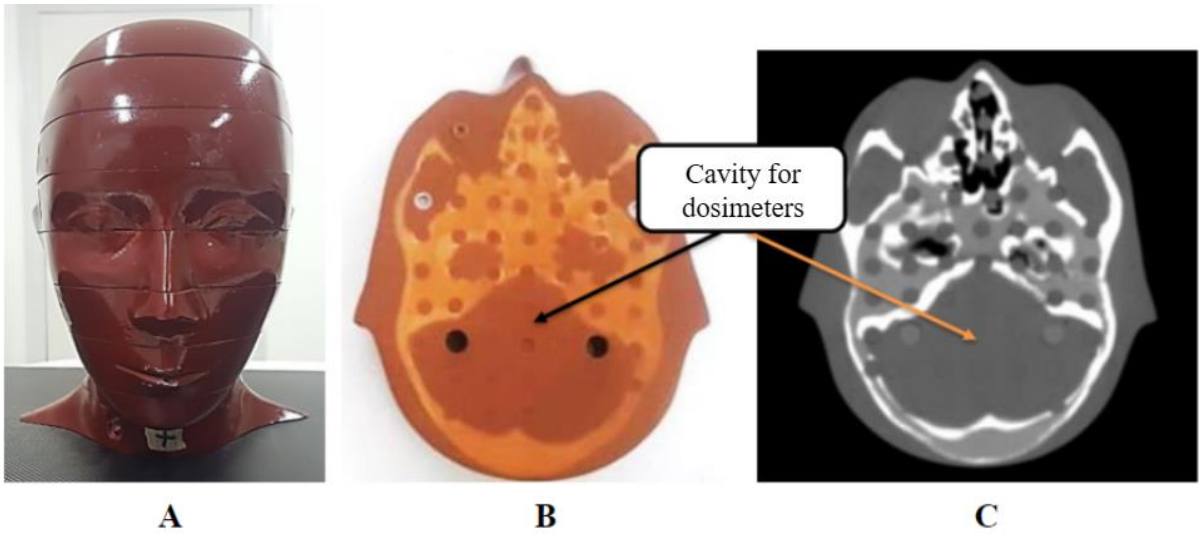

Source: Adapted from Pereira et al [28].

The obtained DICOM file was opened in the 3D Slicer software, where a region of interest between slices 2 and 5 of the ATOM phantom head was defined. The segmentation of the structure based on HU (Fig. 2) was performed to isolate only the regions corresponding to soft tissue. This file was then converted into a three-dimensional digital mesh (OBJ) file and imported into a 3D modeling software for implementing the necessary modifications to accommodate the radiochromic films.

Figure 2: Figure 2: Segmentation panel of the 3D Slicer software. (A) Axial slice; (B) Rendered tomographic pieces; (C) Sagittal slice; (D) Coronal slice.

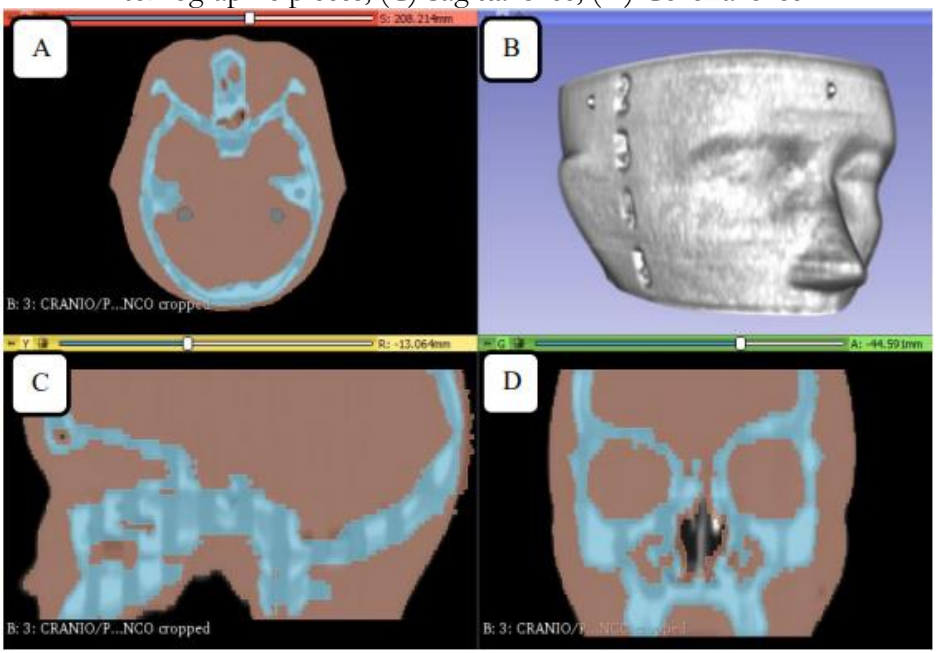

Source: Pereira et al [28].

2.1.2 3D Modeling

The OBJ file obtained from the tomography was imported into the "open-source" software Blender® to model the necessary modifications for accommodating the radiochromic films. At this stage, two new slices were developed in the phantom design to enable dosimetry in horizontal and vertical planes. The first is the axial slice passing through the center of the eyeball and optic nerve. The second slice is oblique and was created perpendicular to the axial plane, running along the path of the optic nerve from the base of the eye to its insertion into the optic foramen of the skull. Thus, the phantom has four distinct pieces (Fig. 3). The radiochromic films can be positioned between the pieces along these two slices. With the correct handling of dosimetric data, it will be possible to achieve a three-dimensional approximation of the dose distribution due to the perpendicularity of the slices.

Figure 3: 3D Model of the Phantom in Blender Software. (A) Complete phantom. The axial slice (red) and oblique slice (blue) are shown. (B) Phantom with the pieces cut by the oblique slice removed. The pieces are represented as superior (1), superior-cut (2), inferior (3), and inferior-cut (4).

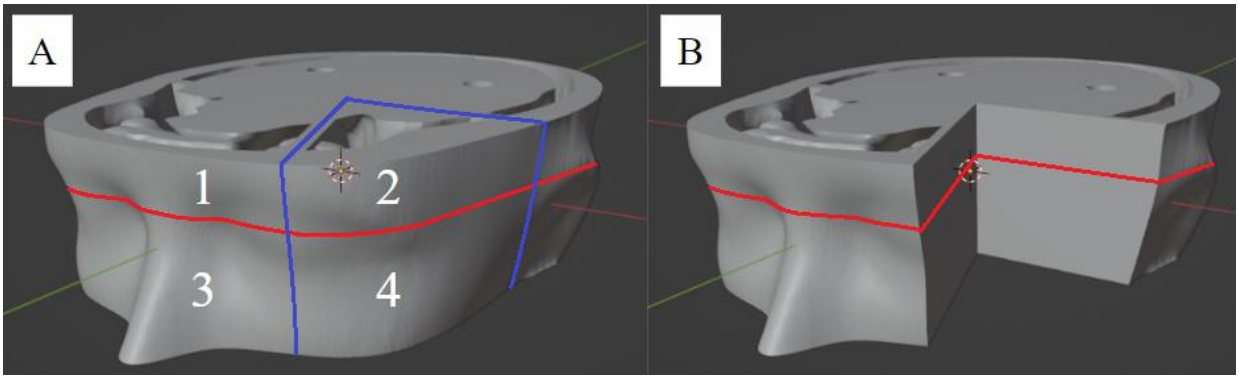

Source: The Author (2024).

2.1.3 3D printing

After modeling in Blender, the files are saved in STL format for printing. The printer used was the 3D Prusa MK3®. It features a heated platform with a print area of 25x21x21 cm^3, prints layers of 0.3 mm, an extruder nozzle with a diameter of 0.4 mm, and is fed with PLA filaments of 1.75 mm diameter [29]. The printing parameters used are listed in Table 1 [26].

Table 1 : Printing parameters.

Printing Parameter	Value
Table temperature	60 °C
Extruder temperature	210 °C
Layer thickness	0.3 mm
Thickness of the initial layer	0.3 mm
Vertical wall layers	2
Layers on horizontal walls	2
Print speed (outer perimeter)	35 mm/s
Print speed (internal infill)	80 mm/s
First layer print speed	20 mm/s
Filling percentage	85%
Infill profile	Rectangular
Infill angle	45°
Extrusion Nozzle Diameter	0.4 mm
Filament diameter	1.75 mm

Source: Pereira et al [26].

The filament used for 3D printing was natural PLA with printing infill of 85%. This choice was based on the material validation discussed by Pereira et al. (2021) [26], which showed less than a 5% difference in mass attenuation coefficient and mass stopping power compared to those established in the literature (PMMA and solid water), as well as similar dose-depth profile to solid water. The filament used was from the company 3DFila.

2.1.4 Bone Tissue Simulation Mixture

To simulate bone tissue, a mixture with volume proportions of 46% CaSO4, 23% H_2O, and 31% NaCl was selected, among other proportions, as it showed discrepancies of less than 2% for the mass attenuation coefficient and mass stopping power for electrons in energies between 1 and 10 MeV. Additionally, it demonstrated compatibility in bulk density and relative electronic density with the ATOM phantom. These results and discussions on the selection of the most suitable proportion for the mixture were reported by Pereira et al. (2022) [27].

Calcium sulfate hemihydrate ($CaSO_4$ + ½ H_2O) is commonly known as gypsum. Practically, this mixture was prepared using conventional gypsum, water, and salt. The materials were placed in a beaker to verify the volume according to the defined proportions. The gypsum and salt were mixed together to ensure homogeneity. Water was then added to create a paste-like mixture to fill the gaps in the 3D printing to form the cranial bones. After preparation and filling, the material needs to be allowed to dry. After approximately one day, the outer parts of the phantom have a dry appearance.

3.1 Validation of the Phantoms

After completing the printing stages, filling the bone portions, and allowing for drying time, it is necessary to verify whether the phantom fulfills its intended purpose: being anthropomorphic and tissue-equivalent. To this end, a CT scan of the constructed phantom was performed to assess homogeneity and HU compatibility with the expected results for bone and soft tissue. Other parameters recommended by ICRU Report 44 were not

evaluated in this work, as the protocol previously validated according to these recommendations was followed [27].

Homogeneity was assessed by taking 50 random points, in both PLA and gypsum, on the phantom's CT scan to check the average HU value and its standard deviation using the 3D Slicer software. The HU value compatibility of PLA was evaluated using the Z statistical test, while the data related to the gypsum mixture were graphically compared with the results from Pereira et al. (2022) [27] to ensure agreement with the materials in the ATOM phantom.

The tomography acquisition was performed on the Philips CT Brilliance Big Bore scanner, installed at Hospital Quinta D'Or, in Rio de Janeiro city. It has a resolution of 2.56 pixels per millimeter and a voxel size of 0.3906 x 0.3906 x 1 mm^3. The institution's standard protocol for head and neck CT scans is 120 kVp, a tube current-time product of 300 mAs, a slice thickness of 1 mm, and an exposure time of 23.5 seconds.

3. RESULTS AND DISCUSSIONS

The anthropomorphic phantom adapted for dosimetry with radiochromic films has been developed (Fig. 4). Figure 4 shows the complete phantom and the interfaces that allow for the positioning of films for dose assessment in ocular structures, such as the optic nerve. Thus, the films need to be cut and placed between these interfaces for the phantom to be irradiated.

Figure 4: Complete anthropomorphic phantom for radiochromic films. (A) Complete phantom. (B) Oblique slice. (C) Superior and inferior pieces divided by the axial slice.

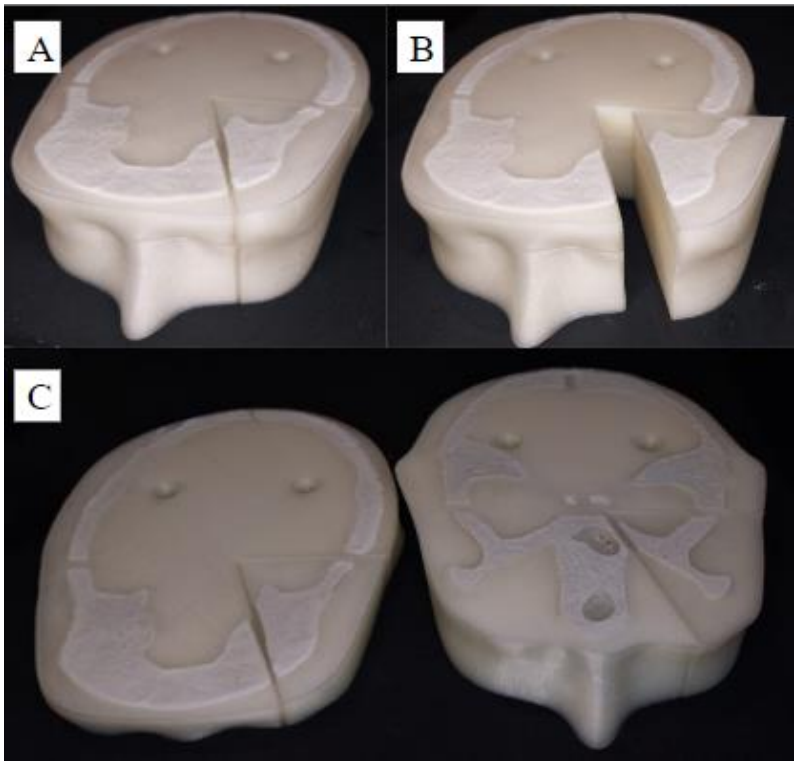

Source: The Author (2024).

The holes present in the posterior portion of both phantoms are necessary for attachment to other pieces of the ATOM phantom. Approximately 30 hours were required for printing the pieces. Regarding the gypsum mixture, it was observed that the outermost part dried after a few hours. However, the waiting time to ensure reliable drying for handling was approximately 72 hours. Nonetheless, it was necessary to keep the phantom in a sealed environment with silica gel to control humidity. The replacement of the pieces in the ATOM is shown (Fig. 5). The most relevant care with the phantom is the fixation and joining of the smaller pieces, which can be ensured with adhesive tape. Thus, for future work, it would be interesting to explore the possibility of adding a horizontal dovetail joint to the pieces for better fixation.

Figure 5: Phantom constructed to replace slices 3 and 4 of the ATOM.

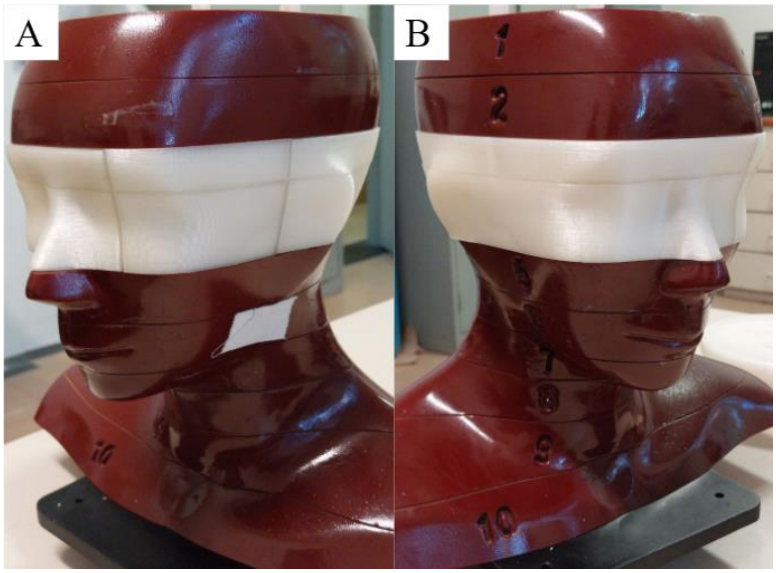

Source: The Author (2024).

The tomographic image of the phantom was viewed in the 3D Slicer software (Fig. 6A and 6B). The bone filling throughout the phantom is observed, as well as the cavities corresponding to the nasal fossae and those intended for positioning the fixation rods for the slices in the ATOM phantom. Figures 6C and 6D show the 3D reconstruction performed in 3D Slicer of the bone filling within the printed piece. This image was obtained by segmenting based on the HU difference between tissues.

Figure 6: Coronal (A) and axial (B) tomographic slices of the complete phantom. Oblique (C) and superior (D) views of the 3D reconstruction in 3D Slicer of the bone portion within the print.

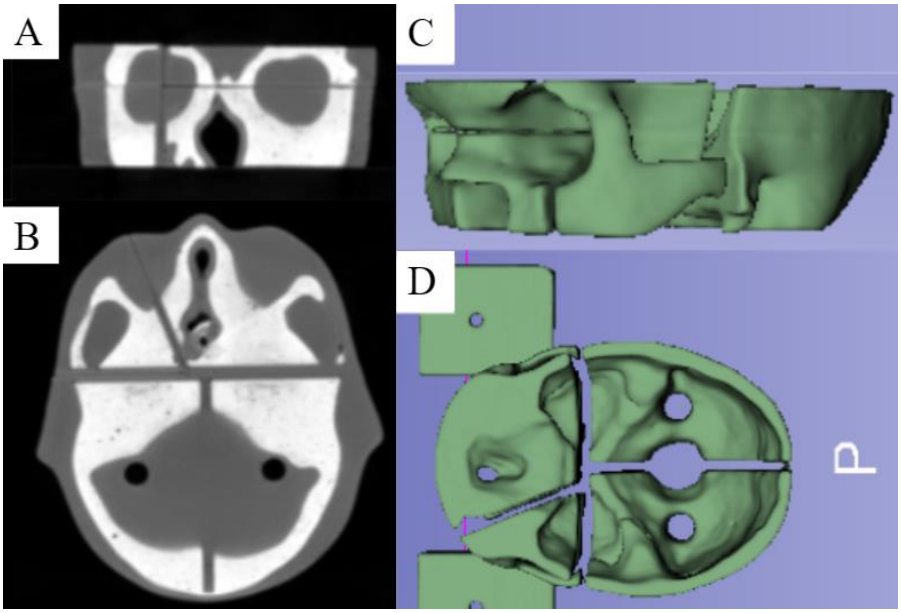

Source: The Author (2024).

3.1 Hounsfield Units analysis

Figure 7 presents the HU graphs for each of the 50 random points along the tomographic slices of the phantom for the gypsum mixture, along with the reference data. The reference data contain the HU values for the bony portion of the ATOM phantom and the gypsum mixtures tested by Pereira et al. (2022) [27].

Since the reference values are presented graphically, their compatibility analysis using the Z test was not feasible. Instead, it was performed visually by comparing the graphs on the same scale. The obtained data demonstrate HU values in the constructed phantom ranging between 1000 and 1500, like the reference data. Thus, its validation can be assured.

Given that HU values can be highly variable with the imaging technique used, validation from these data was possible through the consistency of the technique in tomography. Points that deviate significantly from the average in the bone mixture likely arise from impurities in the materials used for its preparation.

Figure 7: Left - HU graph for the gypsum mixture in the phantom. The mean is represented by the red line. Right - Reference data [27].

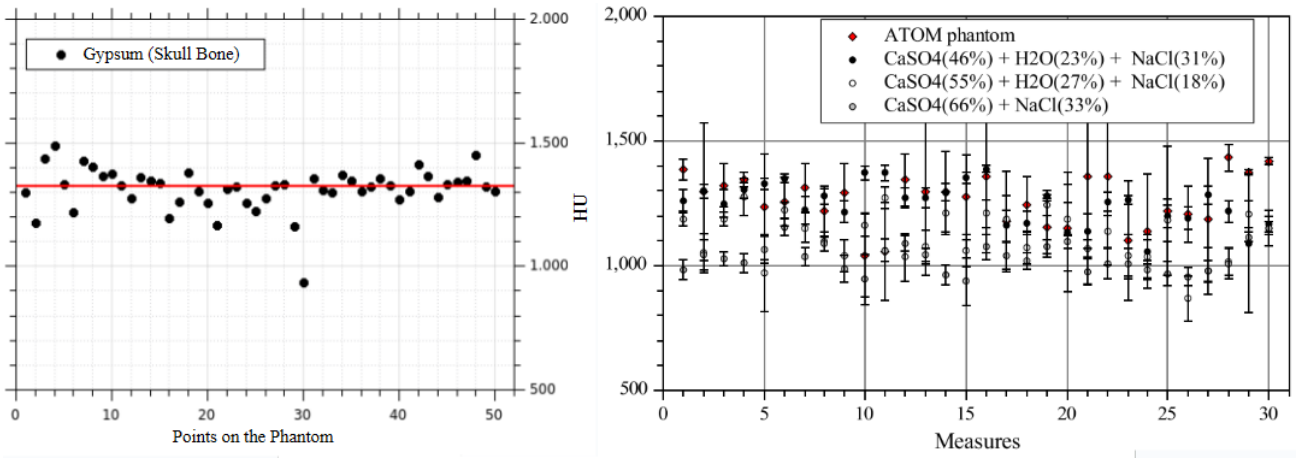

Source: The Author (2024).

Figure 8 presents the HU graph for each of the 50 random points along the tomographic slices of the phantom for the portion printed in PLA. From these data, the mean, standard deviation, and coefficient of variation of these samples were calculated (Table 2). It is believed that this coefficient of variation of 28.1% arises from the absorption of water present in the gypsum mixture by the PLA at varying levels in each portion of the phantom.

Figure 8: HU graph for the PLA portion of the phantoms. The mean is represented by the red line.

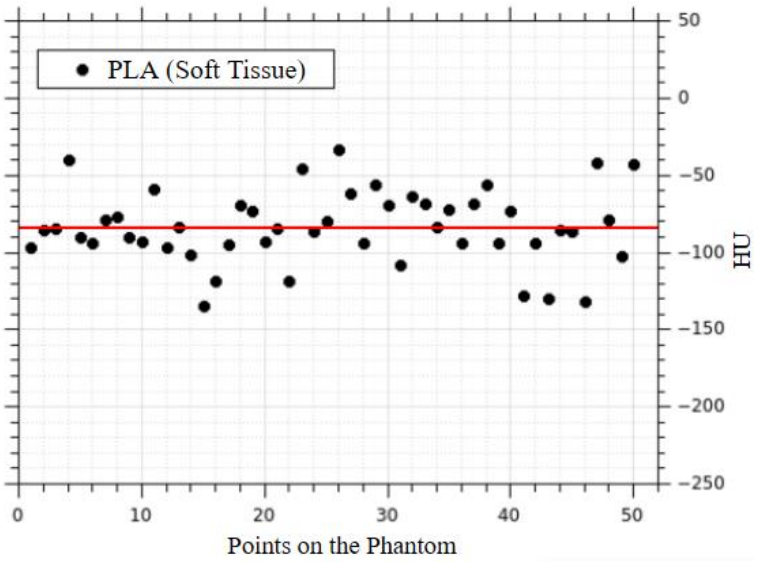

Source: The Author (2024).

Table 2: Homogeneity Analysis Parameters of the Phantom.

Phantom region	Mean HU ± Std. deviation	Coef. of variation (%)
PLA (Soft Tissue)	-85 ± 24	28.1
Gypsum (Skull Bone)	1326 ± 88	6.6

Source: The Author (2024).

The compatibility analysis with the reference values (-30 ± 20) [27] for the HU values in PLA using the Z statistical test demonstrates compatibility within 3σ (Eq. 1).

$$\frac{|(-85)-(-30)|}{\sqrt{24^2+20^2}} = 1.8 \leq 3 \qquad \text{(Eq. 1)}$$

It is important to highlight that the HU values obtained are compatible with the ones measured before for the phantom developed in previous work [27] that was printed using the same PLA. It is known that environmental factors such as humidity play a vital role in the environmental degradation process of PLA. It is important to be attentive to the degradation of the PLA's properties over time.

CONCLUSIONS

The new phantom for dosimetry with radiochromic films was designed to accommodate these dosimeters in both an axial plane and along an oblique cut through the optic nerve. This geometry fulfills the objective and can be tested as a dosimetric system for evaluating continuous dose distributions in the ocular region and its adjacent OARs. This phantom offers an advantage over those using microcube TLDs due to the operational difficulties associated with handling such dosimeters. HU analysis confirmed the homogeneity and compatibility of the developed materials with those of the ATOM® phantom. Homogeneity in HU values was validated by the coefficient of variation, with 28.1% for 3D printing (soft tissue) and 6.6% for the gypsum mixture (bone tissue). Compatibility within 3σ of the HU values in PLA of the created phantom with the ATOM

was also confirmed by the Z test. Additionally, the qualitative graphical analysis of HU values for the gypsum mixture compared with the expected values further supports its validation.

FUNDING

This research was supported by the Conselho Nacional de Desenvolvimento Científico e Tecnológico (CNPq) and the Fundação Carlos Chagas Filho de Amparo à Pesquisa do Estado do Rio de Janeiro (FAPERJ). We gratefully acknowledge their contributions and support, which made this work possible.

CONFLICT OF INTEREST

All authors declare that they have no conflicts of interest.

REFERENCES

[1] CHENG, C. Y.; HSU, Wen-Ming. Incidence of eye cancer in Taiwan: an 18-year review. **Eye**, v. 18, n. 2, p. 152-158, 2004.

[2] KALIKI, S.; SHIELDS, C. L. Uveal melanoma: relatively rare but deadly cancer. **Eye**, v. 31, n. 2, p. 241-257, 2017.

[3] AHMAD, S. M.; ESMAELI, B. Metastatic tumors of the orbit and ocular adnexa. **Current opinion in ophthalmology**, v. 18, n. 5, p. 405-413, 2007.

[4] SHIELDS, J. A.; SHIELDS, C. L.; SCARTOZZI, R. Survey of 1264 patients with orbital tumors and simulating lesions: The 2002 Montgomery Lecture, part 1. **Ophthalmology**, v. 111, n. 5, p. 997-1008, 2004.

[5] LUCENA, E. et al. Epidemiology of uveal melanoma in Brazil. **International Journal of Retina and Vitreous**, v. 6, p. 1-8, 2020.

[6] RIBEIRO, K. C. B.; ANTONELI, C. B. G. Trends in eye cancer mortality among children in Brazil, 1980–2002. **Pediatric blood & cancer**, v. 48, n. 3, p. 296-305, 2007.

[7] THOMSON, R. M. et al. AAPM recommendations on medical physics practices for ocular plaque brachytherapy: report of task group 221. **Medical Physics**, v. 47, n. 5, p. e92-e124, 2020.

[8] CHIU-TSAO, S. et al. Dosimetry of 125I and 103Pd COMS eye plaques for intraocular tumors: Report of Task Group 129 by the AAPM and ABS. **Medical physics**, v. 39, n. 10, p. 6161-6184, 2012.

[9] STANNARD, C. et al. Radiotherapy for ocular tumours. **Eye**, v. 27, n. 2, p. 119-127, 2013.

[10] MUNIER, F. L. et al. New developments in external beam radiotherapy for retinoblastoma: from lens to normal tissue-sparing techniques. **Clinical & experimental ophthalmology**, v. 36, n. 1, p. 78-89, 2008.

[11] JEGANATHAN, V. S. E.; WIRTH, A.; MACMANUS, M. P. Ocular risks from orbital and periorbital radiation therapy: a critical review. **International Journal of Radiation Oncology* Biology* Physics**, v. 79, n. 3, p. 650-659, 2011.

[12] DURKIN, S. R. et al. Ophthalmic and adnexal complications of radiotherapy. **Acta ophthalmologica Scandinavica**, v. 85, n. 3, p. 240-250, 2007.

[13] SCOCCIANTI, S. et al. Organs at risk in the brain and their dose-constraints in adults and in children: a radiation oncologist's guide for delineation in everyday practice. **Radiotherapy and Oncology**, v. 114, n. 2, p. 230-238, 2015.

[14] ABOUAF, L. et al. Standard-fractionated radiotherapy for optic nerve sheath meningioma: visual outcome is predicted by mean eye dose. **International Journal of Radiation Oncology* Biology* Physics**, v. 82, n. 3, p. 1268-1277, 2012.

[15] BUTSON, M. J. et al. Measurement of radiotherapy superficial X-ray dose under eye shields with radiochromic film. **Physica Medica**, v. 24, n. 1, p. 29-33, 2008.

[16] CARINOU, E. et al. Eye lens monitoring for interventional radiology personnel: dosimeters, calibration and practical aspects of Hp (3) monitoring. A 2015 review. **Journal of Radiological Protection**, v. 35, n. 3, p. R17, 2015.

[17] STOLARCZYK, L. et al. Assessment of undesirable dose to eye-melanoma patients after proton radiotherapy. **Radiation measurements**, v. 45, n. 10, p. 1441-1444, 2010.

[18] HASANZADEH, H.; ABEDELAHI, A. Introducing a simple tissue equivalent anthropomorphic phantom for radiation dosimetry in diagnostic radiology and radiotherapy. **Journal of Paramedical Sciences,** v. 2, n. 4, p. 25-29, 2011.

[19] MCGARRY, C. K. et al. Tissue mimicking materials for imaging and therapy phantoms: a review. **Physics in Medicine & Biology**, v. 65, n. 23, p. 23TR01, 2020.

[20] DEWERD, L. A.; KISSICK M. **The phantoms of medical and health physics**. Berlin: Springer, 2014.

[21] WINSLOW, J. F. et al. Construction of anthropomorphic phantoms for use in dosimetry studies. **Journal of Applied Clinical Medical Physics**, v. 10, n. 3, p. 195-204, 2009.

[22] MCGARRY, Conor K. et al. Tissue mimicking materials for imaging and therapy phantoms: a review. **Physics in Medicine & Biology**, v. 65, n. 23, p. 23TR01, 2020.

[23] ICRU. Report 44: Tissue Substitutes in Radiation Dosimetry and Measurement. **Journal of International Commission on Radiation Units and Measurements**, v. 23, 1989.

[24] MADAMESILA, J. et al. Characterizing 3D printing in the fabrication of variable density phantoms for quality assurance of radiotherapy. **Physica Medica**, v. 32, n. 1, p. 242-247, 2016.

[25] KAMOMAE, T. et al. Three-dimensional printer-generated patient-specific phantom for artificial in vivo dosimetry in radiotherapy quality assurance. **Physica Medica**, v. 44, p. 205-211, 2017.

[26] PEREIRA, D. D. et al. Validation of polylactic acid polymer as soft tissue substitutive in radiotherapy. **Radiation Physics and Chemistry**, v. 189, p. 109726, 2021.

[27] PEREIRA, D. D. et al. Development of an anthropomorphic phantom based on 3D printing for assessment of dose delivered to the eye and adjacent tissues. **Radiation Physics and Chemistry**, v. 199, p. 110292, 2022.

[28] PEREIRA, D. D. Desenvolvimento de um simulador antropomórfico baseado em impressão 3D para dosimetria em radioterapia de olho. **Dissertação (mestrado) - Instituto de Radioproteção e Dosimetria**, Rio de Janeiro, 2021.

[29] Prusa Research. Original Prusa i3 MK3S. 2019. Disponível em: https://www.prusa3d.com/category/original-prusa-i3-mk3s/. Acesso em: 10 de Junho de 2024.

LICENSE